I&EC research
Industrial & Engineering Chemistry Research

Article

pubs.acs.org/IECR

Size-Dependent Fluoride Removal Performance of a Magnetic Fe_3O_4@Fe−Ti Adsorbent and Its Defluoridation in a Fluidized Bed

Chang Zhang, Yingzhen Li, Yanping Jiang, and Ting-Jie Wang*

Department of Chemical Engineering, Tsinghua University, Beijing 100084, China

Supporting Information

ABSTRACT: A magnetic Fe_3O_4@Fe−Ti composite nanoadsorbent was aggregated to micrometer size for high-efficiency fluoride removal and effective separation of the adsorbent from the water after defluoridation. The adsorption and separation performances of the micrometer-sized adsorbent were investigated. The granular adsorbent at an aggregated size of approximately 10 μm had little intragranule diffusion resistance. This granule adsorbent was easily separated from water using magnetic separation after defluoridation. The thermal treatment at the best temperature, 200 °C, increased the granular strength without causing the undesired effects of magnetization decrease and crystallinity increase. For the adsorbent granules with an average size of 11 μm that were heated at 200 °C for 1.5 h, the fluoride adsorption was completely achieved within only 2 min in a novel defluoridation process with a fluidized bed, and over 99% of the adsorbent was intercepted by using a magnetic separation unit. After a simple ultrafiltration unit, no adsorbent residue was detected in the outlet water, guaranteeing the safety of the drinking water. Compared with a traditional fixed-bed process, the fluidized-bed process in this work has the advantages of high defluoridation rate, small apparatus size, high security, and suitability for household utilization.

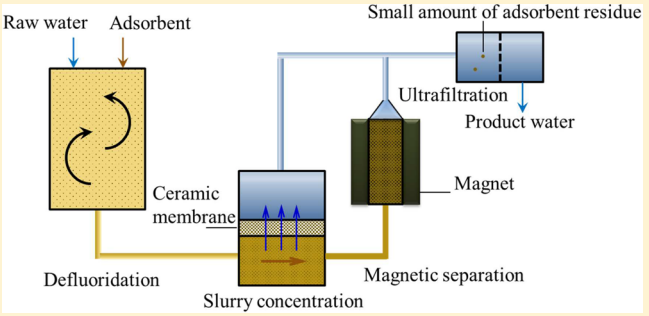

1. INTRODUCTION

Excessive fluoride in drinking water has been a serious threat to human health in many developing countries.[1,2] Water containing high fluoride should be defluorinated before drinking. Among various defluoridation methods, adsorption is the most widely used process because of its easy operation, low cost, and high efficiency.[2,3] Metal oxide adsorbents are effective for fluoride removal.[2−4] Various types of metal oxides have been confirmed to have an excellent affinity to fluoride, such as the oxides of Fe,[5,6] Ti,[7,8] Al,[9,10] Zr,[11] Mg,[12,13] rare earth metals,[4] and so on.[14,15] Compared with conventional bulky adsorbents, nanometer-sized adsorbents have attracted more interest because of their higher area-to-volume ratio, which contributes to a higher adsorption capacity and adsorption rate.[16,17] However, efficient separation of nanoadsorbents from water is difficult. The nanoparticle residue in water causes secondary pollution and threatens the safety of drinking water.[18]

To make use of the high capacity of the nanoadsorbents, the nanoadsorbents were usually granulated to millimeter-sized pellets or granules, which were usually larger than 0.5 mm.[19] For the adsorption using the granules in a packed bed, the granule separation from water is not a problem. However, the large granules have low specific surface area and high intragranule diffusion resistance, leading to a significant loss of adsorption capacity and low adsorption rate. Moreover, organic or inorganic binders are usually used in the granulation of millimeter-sized adsorbent to increase the granule strength, which cover a significant amount of adsorption active sites,[20−22] resulting in an adsorption capacity decrease. The low adsorption rate and capacity result in large equipment size requirements and cause low defluoridation efficiency,[23] which is inconvenient for the dispersed water consumers in rural areas.

For the dispersed water consumers, a safe, rapid, and efficient defluoridation method is desired. To make full use of the high adsorption efficiency of nanoadsorbents, an adsorption process using a solid−liquid fluidized bed with the nanoadsorbents is an ideal method, but efficient separation of nanoadsorbents from water needs to be realized.[19,24] In the fluidized bed, the particle size and driving forces, such as gravity, centrifugal force, and magnetic force, affect the solid−liquid separation efficiency significantly. The larger the particle size and the stronger the driving forces are, the higher the separation efficiency is. Some researchers combined the adsorbent particles with some magnetic materials, such as Fe_3O_4, by surface coating or physical mixing and used an external magnetic field to enhance the separation of the magnetic composite adsorbents.[25−29] However, the evaluation of the separation efficiency in these reports was usually limited to qualitative feasibility analysis,

Received: October 4, 2016
Revised: February 12, 2017
Accepted: February 14, 2017
Published: February 14, 2017

DOI: 10.1021/acs.iecr.6b03856
Ind. Eng. Chem. Res. 2017, 56, 2425−2432

while specific detection of the nanoadsorbent residue and an exact comparison with water quality guidelines were not reported.

In our previous work,[30] a novel Fe_3O_4@Fe−Ti nanoadsorbent was prepared by coating a high adsorption performance Fe−Ti bimetallic oxide onto the surface of superparamagnetic Fe_3O_4 particles to get a composite adsorbent with both high adsorption performance and high magnetic separability. The nanoadsorbent has a high adsorption capacity and adsorption rate, as well as an excellent superparamagnetic property. However, when the composite nanoadsorbent was dispersed in water, it was found that there was still plenty of residue remaining in the water after 10 min of separation in a strong magnetic field, and the iron concentration in the water was significantly above the upper limit of the drinking water quality standard in China (0.3 mg/L, GB5749-2006). The nanoparticles were hard to thoroughly separate from water even with high magnetic assistance. Therefore, the adsorption using nanoadsorbent in a fluidized bed cannot guarantee drinking water safety. To enhance its separability, the nanoadsorbent had to be aggregated to a larger size. Meanwhile, unchanged adsorption performance was desired.

In this work, the Fe_3O_4@Fe−Ti nanoadsorbent was aggregated to get micrometer-sized magnetic adsorbent for high adsorption performance. The adsorption performance and magnetic separability of differently sized Fe_3O_4@Fe−Ti adsorbents for fluoride removal were studied. The granular size and thermal treatment temperature were adjusted for high separation efficiency of the adsorbent from water, high adsorption capacity, and high adsorption rate. By using the best adsorbent, high adsorption and separation efficiency were achieved. The adsorption efficiency was comparable to the initial nanoadsorbent, and no adsorbent residue in the product was detected.

2. EXPERIMENTAL SECTION

2.1. Preparation of Magnetic Adsorbent. A facile coprecipitation method was used to prepare the core−shell Fe_3O_4@Fe−Ti nanoadsorbent.[31] First, 0.25 M $FeCl_2{\cdot}4H_2O$ and 0.05 M $FeCl_3{\cdot}6H_2O$ was dissolved in ethanol; then, 12.5 wt % ammonia solution was dropwise titrated into the mixed solution under mechanical agitation until the pH reached 9.0, resulting in a black suspension of Fe_3O_4 nanoparticles. The Fe_3O_4 nanoparticles were collected using a magnet and then redispersed in deionized water for subsequent coating. Thereafter, 0.3 M $FeSO_4{\cdot}7H_2O$ and 0.3 M $Ti(SO_4)_2$ were dissolved in 150 mL of deionized water to prepare a mixed solution. The solution was dropwise titrated into 200 mL of 0.01 g/mL Fe_3O_4 suspension under mechanical agitation, during which the pH was kept at 4.0 by adding 12.5 wt % ammonia solution. The Fe/Ti ratio of the Fe−Ti oxide and the ratio of Fe−Ti oxide to Fe_3O_4 had been adjusted to get a high adsorption performance and a good magnetization in our previous work.[8,30] The core−shell structure of the composite adsorbent ensured the maximum utilization of the surface active sites for fluoride, because the adsorption was based on an ion exchange process between the fluoride and the hydroxyl groups on the surface of the Fe−Ti adsorbent.[8,31] The prepared nanoadsorbent was collected using a magnet and then washed three times with deionized water.

The micrometer-sized adsorbent was obtained by spray drying and a grinding−sieving process. An experimental spray dryer (YC 015, Shanghai Pilotech Instrument & Equipment Co. Ltd., China) was used for the spray drying of the nanoadsorbent suspension. The prepared nanoadsorbents were redispersed in deionized water at a solid concentration of 0.1 g/mL. The suspension was then pumped into the spray dryer at a rate of 20 mL/min. The inlet and outlet air temperature were 200 and 80 °C, respectively. The inner diameter of the spraying nozzle was 1.5 mm. The average size of the granules after spray drying was 11 μm. The larger granules were prepared using a grinding−sieving process. The nanometer-sized particles were collected and dried in an oven at 80 °C for 12 h. The dried cake with millimeter size were then grinded manually and sieved with Tyler meshes, resulting in adsorbent granules with average size of 11, 28, 97, and 264 μm, as shown in Table S1.

To increase the granule strength, the granules obtained by spray drying or sieving were put in a muffle furnace and heated for 1.5 h at a set temperature. The obtained micrometer-sized adsorbents were used for the following characterizations and experiments.

2.2. Characterizations. The crystalline structure of the adsorbent was analyzed using an X-ray diffraction analyzer (XRD, D8-Advance, Bruker, Germany) over a range of 10−90° with Cu Kα radiation at a scan speed of 5°/min. The average size of the micrometer-sized adsorbent was measured using a Malvern laser analyzer (Mastersizer 3000, Malvern, U.K.). The specific surface area of the adsorbent was measured by nitrogen adsorption with an Autosorb-iQ2-C instrument (Quantachrome Instruments, United States). The magnetism of the adsorbent was analyzed by a vibrating sample magnetometer (VSM, 7307, Lake Shore, United States). The adsorbent residue, Fe and Ti, in water were measured using polarized Zeeman atomic adsorption spectroscopy (AAS, Z-5000, Hitachi High-Technologies Corp., Japan) and inductively coupled plasma atomic emission spectroscopy (ICP-AES, Vista-MPX, VARIAN, United States), respectively.

2.3. Adsorption Performance. The adsorption performance of the micrometer-sized adsorbents was measured through batch experiments. A total of 50 mg of micrometer-sized adsorbent was added to 50 mL of fluoride-containing water with a set F^- concentration in a conical flask. The fluoride solution was prepared by dissolving NaF in deionized water. The pH values of the solutions were in the range of 7−8. For the measurement of the equilibrium adsorption capacity, the flask was put in a thermostat shaker at 180 rpm and 25 °C for 2 h or longer. For the measurement of the adsorption kinetics, a series of flasks were filled with the fluoride solution at the same concentration and adsorbent dosage and were shaken for different set times. The adsorbent was separated from water by putting the flask on a magnet for 5 min. The equilibrium fluoride concentration of the supernatant was measured using a fluoride electrode (PF1, Shanghai KANGYI Instrument Co. Ltd., China) and a fluoride ion meter (PXS-450, Shanghai KANGYI Instrument Co. Ltd., China). Then, the equilibrium adsorption capacity was calculated

$$q_e = \frac{C_0 - C_e}{m/V} \tag{1}$$

where q_e is the equilibrium adsorption capacity (mg/g); C_0 and C_e are the initial and equilibrium fluoride concentrations, respectively (mg/L); m is the mass of adsorbent (g); V is the solution volume (L).

2.4. Magnetic Separation. The magnetic separation experiments were conducted using a 50 × 50 × 10 mm^3

DOI: 10.1021/acs.iecr.6b03856
Ind. Eng. Chem. Res. 2017, 56, 2425−2432

square Nd−Fe−B magnet (N30). The parameters of the magnet were remanence, 1.08−1.12 T; coercivity, 9.8−10.5 kOe; and maximum energy product, 28−30 MGOe.

To examine the magnetic separation efficiency, 50 mg of adsorbent was added to 50 mL of deionized water in a 100 mL flask. The flask was put on a magnet for adsorbent separation for 5 min, and then 5 mL of the supernatant was sampled. Then, 2 mL of 10 wt % sulfuric acid was added to the sample. The mixed solution was kept for 2 h for completely dissolving the solid residue. Then the mixed solution was transferred to a volumetric flask and diluted to 10 mL using deionized water. A blank sample was prepared for reference by diluting 2 mL of 10 wt % sulfuric acid to 10 mL using deionized water. The Fe concentrations of the experimental and blank samples were measured using polarized Zeeman atomic adsorption spectroscopy (AAS, Z-5000, Hitachi High-Technologies Corp., Japan). The Fe concentration in the water after magnetic separation was calculated from the difference between the experimental and blank values.

The iron concentration in the water is the residue of the adsorbent in water. According to the measurement procedure, the measured iron concentration consists of both solid and dissolved residue states. However, because our experiments showed that the dissolving of the adsorbent particles was not detected in the fluoride-containing water at low concentration, e.g., 4.7 mg/L, in the defluoridation process after ultrafiltration, the measured iron concentration in this study can be regarded as solid residue. Low iron concentration represents low adsorbent residue in the water, indicating high magnetic separation efficiency.

2.5. Defluoridation Process of the Micrometer-Sized Magnetic Adsorbent. A novel defluoridation process for the application of the micrometer-sized magnetic adsorbent with high adsorption rate, adsorption capacity, and magnetic separation efficiency is illustrated in Figure 1.

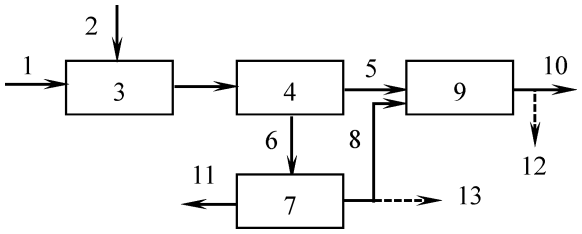

Figure 1. Defluoridation flow sheet using the micrometer-sized magnetic adsorbent and a fluidized bed: 1, raw water; 2, adsorbent; 3, fluidized bed; 4, membrane concentration; 5, defluorided water; 6, concentrated slurry; 7, magnetic separation; 8, defluorided water; 9, ultrafiltration; 10, product water; 11, adsorbent for regeneration; 12, product water sampling port; 13, separated water sampling port.

The continuous defluoridation is conducted via a fluidized bed mixing, ceramic membrane concentration, magnetic separation, and security ultrafiltration. The fluoride-containing water and adsorbent were fed continuously into the fluidized bed and mixed fully for defluoridation. The slurry in the fluidized bed was pumped in a cyclic pattern to ensure a full mixing of the adsorbent and the fluoride solution, thus realizing a high adsorption rate. The well-mixed slurry was transferred into a ceramic membrane with a sieving size of approximately 200 nm. The ceramic membrane concentrates the slurry using a cross-flow pattern. About 90% of the defluorinated water was extracted out and sequentially went to a security ultrafiltration with a sieving size of approximately 10 nm. The concentrated slurry went to the magnetic separation unit, where the used adsorbent was captured and the defluorinated water went to the security ultrafiltration unit. After the ultrafiltration, the adsorbent residue in the water was removed completely, guaranteeing the safety of the final product.

The magnetic field in the magnetic separator is generated by two identical permanent Nd−Fe−B magnets (N30), which has the advantages of low operation cost and small size. The 100 × 100 × 10 mm^3 magnets with a remanence of about 1.10 T are mounted face-to-face in an N-to-S pattern, leaving a gap of 20 mm. The concentrated slurry flowed through the gap between the magnets in the perpendicular direction of the magnetic field. Ten pieces of wire mesh sheets (sheet size is 100 × 100 mm^2, wire diameter 0.2 mm, and mesh hole size 1.5 × 1.5 mm^2) are packed in the gap to create a high-gradient magnetic field. Most of the used adsorbent particles were captured by the magnetic separator. The ceramic membrane before magnetic separator concentrates the slurry, contributing to the effective adsorbent particle capture in the magnetic separation. After the magnetic separation, only a very small amount of adsorbent particles are left in the water flow, which will be trapped by the security ultrafiltration. The load of the ultrafiltration is reduced to a very low level due to the high efficiency of the magnetic separation, guaranteeing a long running cycle and a low operation cost.

Compared with the traditional fixed bed process, this process with a fluidized bed has a higher defluoridation efficiency due to the direct use of the micrometer-sized granules and the ideal solid−liquid mixing. The combination of fast defluoridation and efficient adsorbent trapping contributes to fast water production and small apparatus size, making it suitable for household utilization.

In the adsorption experiment, the initial fluoride concentration of the aqueous solution was 4.7 mg/L, which resembled the typical fluoride content of high-fluoride groundwater in China (3−5 mg/L).[32,33] The fluoride solution was prepared by dissolving NaF in deionized water. The pH values of the solutions were in the range of 7−8. The adsorbent dosage was set to 0.5 g/L, and the water flux was approximately 35 L/h. The fluoride removal efficiency and the product water safety were evaluated by measuring the concentration of the fluoride and metal ions in the product water at the product water sampling port in Figure 1. The magnetic separation efficiency, i.e., the ratio of the magnetic-trapped adsorbent amount to the feed adsorbent amount, was determined by measuring the iron residue in the defluorinated water after the magnetic separation unit at the separated water sampling port in Figure 1.

3. RESULTS AND DISCUSSION

3.1. Magnetic Separation Efficiency. The micrometer-sized granular adsorbent with high strength produces little residue in the water and gives a high magnetic separation efficiency. To increase the mechanical strength of the particles against water scouring, the micrometer-sized granular adsorbent with an average size of 11 μm was heated at 100, 200, 300, 400, and 500 °C. The residue in the water after magnetic separation was detected as shown in Table 1. For comparison, the residue in the water for the adsorbent without thermal treatment is also given in Table 1. It is shown that the residue decreased after thermal treatment at all temperatures, indicating that the granule strength increased after thermal treatment. The residue reached a minimum value at 200 °C. It is inferred that the

DOI: 10.1021/acs.iecr.6b03856
Ind. Eng. Chem. Res. 2017, 56, 2425−2432

Table 1. Adsorbent Residue in the Water after Magnetic Separation Using the 11 μm Adsorbent Heated at Different Temperatures[a]

thermal treatment T(°C)	no	100	200	300	400	500
Fe residue (mg/L)	1.10	0.72	0.13	0.25	0.38	0.43

[a]The upper limit for [Fe] in GB5749-2006 is 0.30 mg/L.

magnetization of the micrometer-sized granular adsorbent changed after thermal treatment. Figure 2 shows that the magnetization of the micrometer-sized adsorbent decreased significantly with the increase of thermal treatment temperature, which led to the residue increase. The dual influence of thermal treatment on granule strength and magnetization resulted in the change of the residue. Therefore, 200 °C was set as the best temperature for the thermal treatment to produce high magnetic separation efficiencies of the adsorbent.

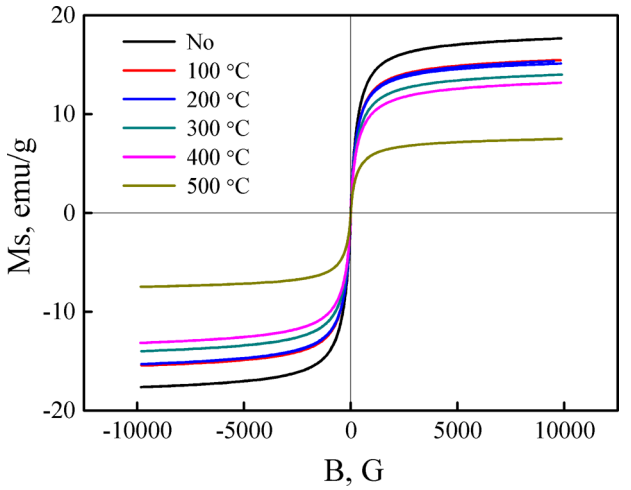

Figure 2. Magnetization of the 11 μm magnetic adsorbent at different thermal treatment temperatures.

To investigate the size influence of the micrometer-sized granular adsorbent on magnetic separation efficiency, the residue in the water using different micrometer-sized granular adsorbent after being heated at 200 °C was detected, as shown in Table 2. It is shown that the residues of micrometer-sized adsorbents in the water were much lower than that of nanometer-sized adsorbents. When using the micrometer-sized granular adsorbent in the size range of 11−97 μm, the residue in the water met the guidelines for drinking water quality in China. However, as the granule size increased to 264 μm, the magnetic separation efficiency decreased sharply, which is a result of the increase in the granule abrasion due to the larger size. For comparison, the residue in the water using granular adsorbent with different sizes without thermal treatment are also given in Table 2. It is shown that all of the adsorbents without thermal treatment had lower separation efficiency. The changing trend of the magnetic separation efficiency with granule size was basically the same as that of the adsorbent heated at 200 °C. It is confirmed that thermal treatment at 200 °C for the micrometer-sized granular adsorbent can increase the magnetic separation efficiency of the magnetic adsorbent in the size range of 11−264 μm.

Table 2. Residue in the Water Using the Nanoadsorbent and the Granular Adsorbent with Different Size after Magnetic Separation[a]

average size		20 nm	11 μm	28 μm	97 μm	264 μm
Fe residue (mg/L)	200 °C thermal treatment	–[b]	0.13	0.23	0.25	1.19
	no thermal treatment	5.10	1.10	1.00	1.00	2.27

[a]The upper limit for [Fe] of GB5749-2006 is 0.30 mg/L. [b]The nanoadsorbent was kept in water; therefore, it was not heated.

Therefore, to achieve high magnetic separation efficiency and ensure drinking water safety, the thermal treatment temperature was set at 200 °C with a granule size of approximately 10 μm.

3.2. Adsorption Capacity. The temperature effects of the thermal treatment on the adsorption capacity of the micrometer-sized granular adsorbent were investigated. The adsorption capacities of the 11 μm adsorbent heated at 100, 200, 300, 400, and 500 °C were measured and compared with the adsorbent without thermal treatment, as shown in Table 3.

Table 3. Adsorption Capacity and Specific Surface Area of the Adsorbent Granules at Different Thermal Treatment Temperatures ($[F^-]_0$ = 50 mg/L)

thermal treatment T (°C)	no	100	200	300	400	500
Q_e (mg/g)	29.1	30.9	29.7	16.3	11.6	8.8
SSA (m^2/g)	106.8	101.5	99.2	72.8	57.3	53.7

When heated at 100 or 200 °C, the adsorption capacity was basically the same as that without thermal treatment. As the temperature increased, the adsorption capacity decreased significantly. This is inferred to be result of the decrease in the specific surface area and active sites, as shown in Table 3.

The XRD spectra of the micrometer-sized granular adsorbent heated at different temperatures was measured, as shown in Figure 3. The characteristic peaks of Fe_3O_4 (PDF entry 99-0073) in all of the spectra were similar. When the thermal treatment temperature increased, the characteristic peak of TiO_2 (PDF entry 29-1360) at 25.6° became significantly stronger, which indicates that the adsorptive component in the composite adsorbent changed from amorphous to crystalline

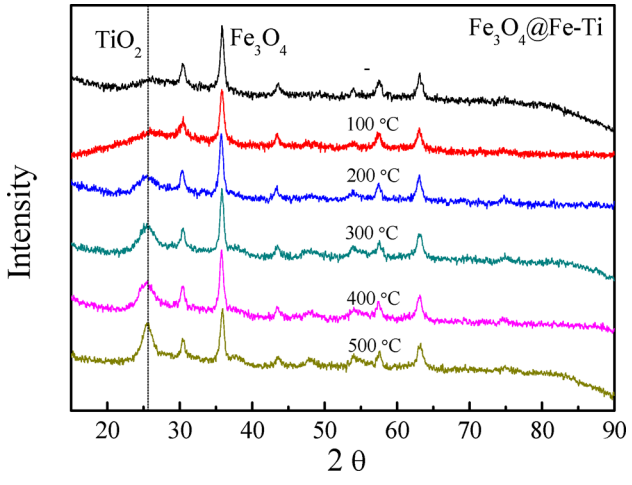

Figure 3. XRD spectra of the micrometer-sized granular adsorbent at different thermal treatment temperatures.

DOI: 10.1021/acs.iecr.6b03856
Ind. Eng. Chem. Res. 2017, 56, 2425−2432

after high-temperature thermal treatment, causing the decrease of the adsorption capacity.

To investigate the adsorption capacity of different micrometer-sized adsorbents, the equilibrium adsorption capacity of the micrometer-sized adsorbents and nanoadsorbent was measured at the initial fluoride concentration of 50 mg/L. The micrometer-sized adsorbents were heated at 200 °C. As shown in Table 4, different micrometer-sized adsorbents had

Table 4. Equilibrium Adsorption Capacity and Specific Surface Area of the Micrometer-Sized Adsorbents

average size	20 nm	11 μm	28 μm	97 μm	264 μm
Q_e (mg/g)	32.5	29.7	32.5	28.5	28.3
SSA (m^2/g)	–[a]	99.2	95.3	102.1	107.2

[a]The nanoadsorbent was maintained in water, and its specific surface area was not measured.

almost the same adsorption capacity as the nanoadsorbent, indicating that the micrometer-sized granular adsorbent maintained the high adsorption capacity. The specific surface area of the granular adsorbents was determined by nitrogen adsorption. Table 4 shows that the specific surface areas of the granular adsorbents for different sizes were almost the same, confirming that the loss of the adsorption surface active sites was small and the adsorption capacity was not changed.

It showed that the micrometer-sized granular adsorbent had nearly the same adsorption capacity as the nanoadsorbent, and the micrometer-sized adsorbent kept the high adsorption capacity after the micrometer-sized granular adsorbent was heated at 200 °C.

3.3. Adsorption Rate. According to the above results, 200 °C was set as the best temperature of the thermal treatment for high magnetic separation efficiency and high adsorption capacity. The adsorption rates of the 11 μm adsorbent heated at 200 °C and without thermal treatment were measured. The adsorption data were fitted using the first- and second-order kinetic models

$$\frac{dq}{dt} = k_1(q_e - q) \quad (2)$$

$$\frac{dq}{dt} = k_2(q_e - q)^2 \quad (3)$$

After integration, the adsorption capacities are

$$q = q_e(1 - e^{-k_1 t}) \quad (4)$$

$$q = k_2 q_e^{\ 2} t/(1 + k_2 q_e t) \quad (5)$$

where k_1 and k_2 are the rate constants of the first- and second-order kinetic models, respectively; q_e is the equilibrium adsorption capacity, and q is the adsorption capacity at time t. For simplification, the time t_{95} at $q = 0.95q_e$ was used to evaluate the apparent adsorption rate. The fitting results showed that both first- and second-order kinetic models fitted well with experimental data. The experimental data and fitted curves using the second-order kinetic model are shown in Figure 4. The fitted parameters are shown in Table S2. Table S2 shows that the rate constant with 200 °C thermal treatment was lower than that without treatment, but the time t_{95} for both adsorbents was less than 1 min, indicating a high apparent adsorption rate from a practical viewpoint.

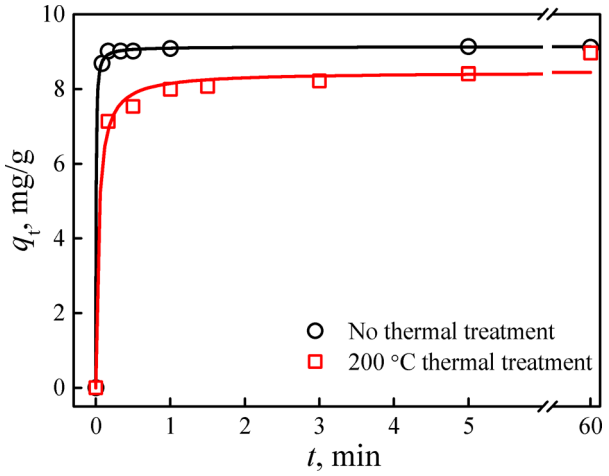

Figure 4. Adsorption data and fitted curves for the adsorbents with and without thermal treatment using the second-order kinetic model (the average size is 11 μm; $[F^-]_0$ = 10 mg/L).

To investigate the influence of granular adsorbent size on adsorption rate, the adsorption rate of different micrometer-sized adsorbent heated at 200 °C was measured. The adsorption data fitted with the second-order kinetic model are shown in Figure 5. The fitted parameters using the first- and

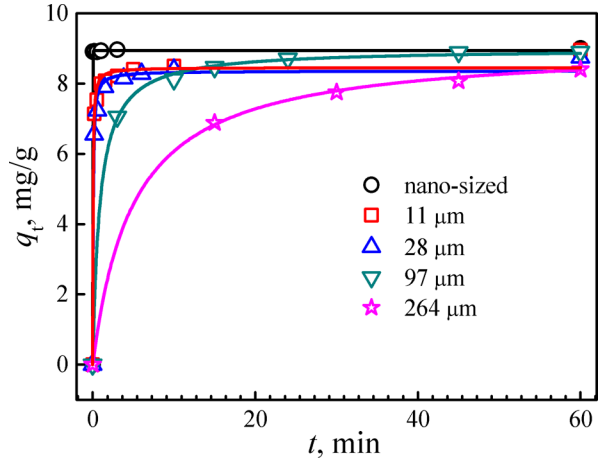

Figure 5. Adsorption data and fitted curves using the second-order kinetic model for the nano- and micrometer-sized adsorbents.

second-order kinetic model are listed in Table S3. Table S3 shows that the rate constant decreased significantly as granule size increased, indicating the increase of intraparticle diffusion resistance. For adsorbent granules not larger than 28 μm, t_{95} was less than 1 min, while for the 97 μm granular adsorbent, t_{95} was 16.3 min, which indicates a much lower adsorption rate using the second-order kinetic model.

Therefore, a high adsorption rate can be achieved using the granular adsorbent in a size range of 11–28 μm. Taking into account magnetic separation efficiency, adsorption capacity, and adsorption rate, the best granule size is 11–28 μm, and the best thermal treatment temperature is 200 °C.

3.4. Intraparticle Diffusion. To investigate the intraparticle diffusion of the micrometer-sized adsorbents during the adsorption process, the adsorption data were fitted with the intraparticle diffusion model proposed by Weber and Morris[34,35]

DOI: 10.1021/acs.iecr.6b03856
Ind. Eng. Chem. Res. 2017, 56, 2425–2432

$$q_t = k_d t^{1/2} + C \quad (6)$$

where q_t is the adsorption capacity at time t, k_d the diffusion rate constant, and the intercept C a constant related to the boundary layer effect. If the curve of q_t versus $t^{1/2}$ is linear and passes through the origin, then intraparticle diffusion is the rate-determining step of adsorption. The larger the intercept C is, the smaller the effect of intraparticle diffusion is on the rate determination.[36]

According to eq 6, the curves of q_t versus $t^{1/2}$ were fitted in two separate sections that represent a quick adsorption section and a near-equilibrium section, as is shown in Figure 6. The

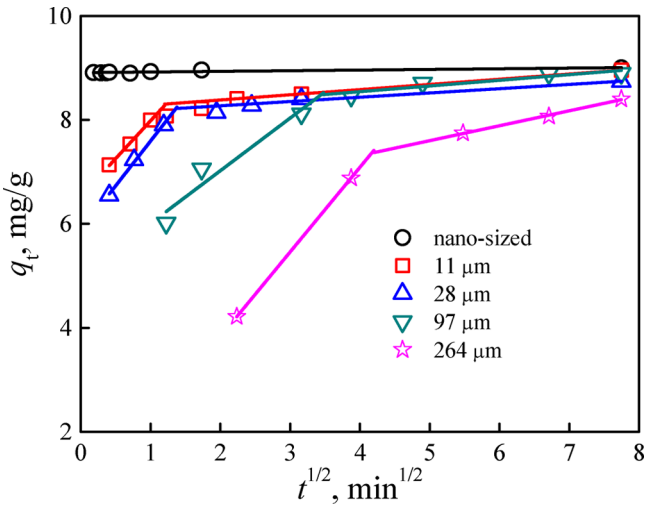

Figure 6. Intraparticle diffusion model fitting for the nano- and micrometer-sized adsorbents.

quick section has an apparently high adsorption rate, and the near-equilibrium section has an apparently low adsorption rate. For the nanoadsorbent, the adsorption reached equilibrium immediately; thus, there was almost no quick adsorption section. For all micrometer-sized granular adsorbents, the fitted lines did not pass through the origin, and the intercepts of the quick adsorption section were different. Basically, smaller granules have larger intercepts, indicating less intraparticle diffusion. When the granule is not larger than 28 μm, the intraparticle diffusion is minor. The fitted parameters are shown in Table S4.

3.5. Defluoridation in a Novel Process with a Fluidized Bed. To examine the practical defluoridation efficiency of the best micrometer-sized adsorbent, a novel process with a fluidized bed for rapid defluoridation was designed. The flow sheet of the defluoridation process is shown in Figure 1. The granular adsorbent with an average size of 11 μm after 200 °C thermal treatment was used. The Langmuir saturation adsorption capacity was 41.8 mg/g.[31] The feed rate of the fluoride bearing water was 35 L/h, and the volume of the fluidized bed was 1 L, in which the residence time for defluoridation was less than 2 min. The product water at every liter interval was sampled for examination in the continuous defluoridation process. The water parameters and magnetic separation efficiency are listed in Table 5. The fluoride concentration in the product water was reduced from the initial 4.7 mg/L to under 1.0 mg/L in the product. After the magnetic separation, the Fe residue was in the range of 2−5 mg/L, indicating the magnetic separation efficiency was higher than 99%. This means that the magnetic separation can effectively remove almost all of the adsorbents, which greatly reduces the subsequent ultrafiltration load, ensuring a long-term stable running of the defluoridation. After the ultrafiltration, the iron and titanium residue in the product water was lower than the detection limit of the instruments, i.e., 0.01 mg/L for Fe and 0.002 mg/L for Ti, indicating that neither solid residue nor dissolved residue existed in the product water, guaranteeing the safety of the drinking water. The structure and operation parameters of the novel defluoridation process can be designed and optimized according to practical requirements to achieve best performances. The size of the separator, the structure of the wire mesh in the magnetic separator, and the magnetic field strength can be designed to get a higher separation efficiency, and the separator can be operated continuously by alternate running of two magnetic separators. The exhausted adsorbent is collected and regenerated separately.

In summary, the effective practical utilization of the established adsorbent is realized by a novel fluidized-bed defluoridation process. The novel process had high efficiency, low cost, and guaranteed safety. The characteristics of the defluoridation process using a fluidized-bed with micrometer-sized magnetic Fe_3O_4@Fe−Ti adsorbent are analyzed as follows: (1) The micrometer-sized magnetic adsorbents were used to avoid the diffusion control in the adsorption process and achieve an excellent solid−liquid mixing, obtaining a high

Table 5. Fluoride Adsorption Capacity and Magnetic Separation Efficiency of the Novel Defluoridation Process (Flow Rate, 35 L/h)

sampling	F^- adsorption capacity (mg/g)	Fe residue after magnetic separation (mg/L)	magnetic separation efficiency (%)	iutlet F^- concentration (mg/L)	outlet Fe and Ti concentration (mg/L)
1st	7.7	1.5	99.7	0.9	–[a]
2nd	7.7	4.3	99.1	0.9	–
3rd	7.9	4.1	99.2	0.8	–
4th	7.8	4.3	99.1	0.9	–
5th	7.7	5.1	99.0	0.9	–
6th	7.7	4.9	99.0	0.9	–
7th	7.9	4.2	99.2	0.8	–
8th	7.8	3.8	99.2	0.8	–
9th	7.8	3.4	99.3	0.8	–
10th	7.8	2.7	99.5	0.8	–

[a]"–": The data are lower than the detection limit.

DOI: 10.1021/acs.iecr.6b03856
Ind. Eng. Chem. Res. 2017, 56, 2425−2432

defluoridation efficiency, including fast adsorption rate and high adsorption capacity. (2) The preconcentration of the adsorbent slurry in the adsorption process and the following magnetic separation achieved high separation efficiency of the adsorbents and reduced the load of the subsequent ultrafiltration significantly. (3). Because over 99% of the adsorbents have been captured by the magnetic separation, the security ultrafiltration can completely intercept the very small amount of residue adsorbents, even the possible nonmagnetic residues, guaranteeing the safety of product water for drinking. (4) The continuous adsorption process and the short resistance time of the adsorbent and the water in a fluidized bed make it possible for the apparatus to have small size and produce water quickly, which is more suitable for household utilization.

4. CONCLUSION

The micrometer-sized magnetic Fe_3O_4@Fe−Ti adsorbent was used in a novel process with a fluidized bed for fluoride removal from drinking water with results showing a high adsorption capacity, adsorption rate, and magnetic separation efficiency of the adsorbent. Thermal treatment was employed to increase the granule strength and increase the separation efficiency of the adsorbent. However, it also decreased the saturation magnetization and increased the crystallinity of the adsorbent, leading to the decrease in the separation efficiency and the adsorption capacity. The temperature of the thermal treatment was adjusted and set at 200 °C. The granule size had little influence on adsorption capacity, but larger granules have a higher intraparticle diffusion resistance. For a high magnetic separation efficiency and high adsorption rate, the granule size of the magnetic adsorbent was adjusted and set at approximately 10 μm. For the adsorbent granules at approximately 10 μm and heated at 200 °C, the adsorption was completed within 2 min, and the adsorbent was effectively intercepted by a magnetic separation unit. After a security ultrafiltration, safe drinking water was produced.

■ ASSOCIATED CONTENT

Supporting Information

The Supporting Information is available free of charge on the ACS Publications website at DOI: 10.1021/acs.iecr.6b03856.

Average size of the micrometer-sized adsorbent (Table S1) and adsorption kinetic parameters of the adsorbent with different sizes and thermal treatment temperatures (Tables S2−S4) (PDF)

■ AUTHOR INFORMATION

Corresponding Author

*Tel: 86-10-62788993. Fax: 86-10-62772051. E-mail: wangtj@tsinghua.edu.cn.

ORCID

Ting-Jie Wang: 0000-0003-4468-9498

Notes

The authors declare no competing financial interest.

■ ACKNOWLEDGMENTS

The authors express their appreciation for the financial support of this study by the National High Technology Research and Development Program (863 Program, No. 2012AA062605) and the National Natural Science Foundation of China (NSFC No. 21176134).

■ REFERENCES

(1) Ayoob, S.; Gupta, A. K. Fluoride in drinking water: A review on the status and stress effects. *Crit. Rev. Environ. Sci. Technol.* **2006**, *36*, 433.

(2) Bhatnagar, A.; Kumar, E.; Sillanpää, M. Fluoride removal from water by adsorption-A review. *Chem. Eng. J.* **2011**, *171*, 811.

(3) Habuda-Stanić, M.; Ravančić, M.; Flanagan, A. A review on adsorption of fluoride from aqueous solution. *Materials* **2014**, *7*, 6317.

(4) Wu, X.; Zhang, Y.; Dou, X.; Yang, M. Fluoride removal performance of a novel Fe-Al-Ce trimetal oxide adsorbent. *Chemosphere* **2007**, *69*, 1758.

(5) Huang, Y.; Shih, Y.; Chang, C. Adsorption of fluoride by waste iron oxide: the effects of solution pH, major coexisting anions, and adsorbent calcination temperature. *J. Hazard. Mater.* **2011**, *186*, 1355.

(6) Kumar, E.; Bhatnagar, A.; Ji, M.; Jung, W.; Lee, S.-H.; Kim, S.-J.; et al. Defluoridation from aqueous solutions by granular ferric hydroxide (GFH). *Water Res.* **2009**, *43*, 490.

(7) Chen, L.; He, B. Y.; He, S.; Wang, T. J.; Su, C. L.; Jin, Y. Fe-Ti oxide nano-adsorbent synthesized by co-precipitation for fluoride removal from drinking water and its adsorption mechanism. *Powder Technol.* **2012**, *227*, 3.

(8) Chen, L.; He, S.; He, B. Y.; Wang, T. J.; Su, C. L.; Zhang, C.; Jin, Y. Synthesis of iron-doped titanium oxide nano-adsorbent and its adsorption characteristics for fluoride in drinking water. *Ind. Eng. Chem. Res.* **2012**, *51*, 13150.

(9) Zhou, Q.; Lin, X.; Li, B.; Luo, X. Fluoride adsorption from aqueous solution by aluminum alginate particles prepared via electrostatic spinning device. *Chem. Eng. J.* **2014**, *256*, 306.

(10) Du, J. Y.; Sabatini, D. A.; Butler, E. C. Synthesis, characterization, and evaluation of simple aluminum-based adsorbents for fluoride removal from drinking water. *Chemosphere* **2014**, *101*, 21.

(11) Velazquez-Jimenez, L. H.; Hurt, R. H.; Matos, J.; Rangel-Mendez, J. R. Zirconium-carbon hybrid sorbent for removal of fluoride from water: oxalic acid mediated Zr(IV) assembly and adsorption mechanism. *Environ. Sci. Technol.* **2014**, *48*, 1166.

(12) Zhang, K.; Wu, S.; Wang, X.; He, J.; Sun, B.; Jia, Y.; et al. Wide pH range for fluoride removal from water by MHS-MgO/$MgCO_3$ adsorbent: Kinetic, thermodynamic and mechanism studies. *J. Colloid Interface Sci.* **2015**, *446*, 194.

(13) Suzuki, T.; Nakamura, A.; Niinae, M.; Nakata, H.; Fujii, H.; Tasaka, Y. Immobilization of fluoride in artificially contaminated kaolinite by the addition of commercial-grade magnesium oxide. *Chem. Eng. J.* **2013**, *233*, 176.

(14) Srivastav, A. L.; Singh, P. K.; Srivastava, V.; Sharma, Y. C. Application of a new adsorbent for fluoride removal from aqueous solutions. *J. Hazard. Mater.* **2013**, *263*, 342.

(15) Zhu, B. S.; Jia, Y.; Jin, Z.; Sun, B.; Luo, T.; Yu, X. Y.; et al. Controlled synthesis of natroalunite microtubes and spheres with excellent fluoride removal performance. *Chem. Eng. J.* **2015**, *271*, 240.

(16) Xiao, S.; Wu, S.; Shen, M.; Guo, R.; Huang, Q.; Wang, S.; et al. Polyelectrolyte multilayer-assisted immobilization of zero-valent iron nanoparticles onto polymer nanofibers for potential environmental applications. *ACS Appl. Mater. Interfaces* **2009**, *1*, 2848.

(17) Gao, S.; Sun, R.; Wei, Z.; Zhao, H.; Li, H.; Hu, F. Size-dependent defluoridation properties of synthetic hydroxyapatite. *J. Fluorine Chem.* **2009**, *130*, 550.

(18) Tesh, S. J.; Scott, T. B. Nano-composites for water remediation: a review. *Adv. Mater.* **2014**, *26*, 6056.

(19) Chang, C. F.; Lin, P. H.; Höll, W. Aluminum-type superparamagnetic adsorbents: Synthesis and application on fluoride removal. *Colloids Surf., A* **2006**, *280*, 194.

(20) Chen, L.; Wang, T.; Wu, H.; Jin, Y.; Zhang, Y.; Dou, X. Optimization of a Fe-Al-Ce nano-adsorbent granulation process that used spray coating in a fluidized bed for fluoride removal from drinking water. *Powder Technol.* **2011**, *206*, 291.

(21) Chen, L.; Wu, H.; Wang, T.; Jin, Y.; Zhang, Y.; Dou, X. Granulation of Fe-Al-Ce nano-adsorbent for fluoride removal from drinking water by spray coating on sand in a fluidized bed. *Powder Technol.* **2009**, *193*, 59.

DOI: 10.1021/acs.iecr.6b03856
Ind. Eng. Chem. Res. 2017, 56, 2425−2432

(22) Wu, H.; Wang, T.; Chen, L.; Jin, Y.; Zhang, Y.; Dou, X. Granulation of Fe-Al-Ce hydroxide nano-adsorbent by immobilization in porous polyvinyl alcohol for fluoride removal in drinking water. *Powder Technol.* **2011**, *209*, 92.
(23) Sorg, T. J.; Wang, L.; Chen, A. The costs of small drinking water systems removing arsenic from groundwater. *Aqua* **2015**, *64*, 219.
(24) Belessi, V.; Lambropoulou, D.; Konstantinou, I.; Zboril, R.; Tucek, J.; Jancik, D.; et al. Structure and photocatalytic performance of magnetically separable titania photocatalysts for the degradation of propachlor. *Appl. Catal., B* **2009**, *87*, 181.
(25) Ye, M.; Zhang, Q.; Hu, Y.; Ge, J.; Lu, Z.; He, L.; et al. Magnetically recoverable core-shell nanocomposites with enhanced photocatalytic activity. *Chem. - Eur. J.* **2010**, *16*, 6243.
(26) Chai, L.; Wang, Y.; Zhao, N.; Yang, W.; You, X. Sulfate-doped Fe_3O_4/Al_2O_3 nanoparticles as a novel adsorbent for fluoride removal from drinking water. *Water Res.* **2013**, *47*, 4040.
(27) Chang, C.-F.; Chang, C. Y.; Hsu, T. L. Removal of fluoride from aqueous solution with the superparamagnetic zirconia material. *Desalination* **2011**, *279*, 375.
(28) Zhao, X.; Wang, J.; Wu, F.; Wang, T.; Cai, Y.; Shi, Y.; Jiang, G. Removal of fluoride from aqueous media by Fe_3O_4@$Al(OH)_3$ magnetic nano-particles. *J. Hazard. Mater.* **2010**, *173*, 102.
(29) Poursaberi, T.; Hassanisadi, M.; Torkestani, K.; Zare, M. Development of zirconium (IV)-metalloporphyrin grafted Fe_3O_4 nano-particles forefficient fluoride removal. *Chem. Eng. J.* **2012**, *189-190*, 117.
(30) Zhang, C.; Chen, L.; Wang, T. J.; Su, C. L.; Jin, Y. Synthesis and properties of a magnetic core-shell composite nano-adsorbent for fluoride removal from drinking water. *Appl. Surf. Sci.* **2014**, *317*, 552.
(31) Zhang, C.; Li, Y.; Wang, T. J.; Jiang, Y.; Wang, H. Adsorption of drinking water fluoride on a micron-sized magnetic Fe_3O_4@Fe-Ti composite adsorbent. *Appl. Surf. Sci.* **2016**, *363*, 507.
(32) Li, X.; Zhu, L.; Hou, X.; Zhang, L. Distribution and evolutional mechanism of shallow high-fluoride groundwater in Taiyuan basin. *Acta Geosci. Sin.* **2007**, *28*, 55.
(33) Liu, D.; Chen, Q.; Yu, Z.; Yuan, Z. Geochemical problems of endemic fluorosis disease. *Geochimica* **1980**, 13.
(34) Yadav, A. K.; Kaushik, C. P.; Haritash, A. K.; Kansal, A.; Rani, N. Defluoridation of groundwater using brick powder as an adsorbent. *J. Hazard. Mater.* **2006**, *128*, 289.
(35) Sairam Sundaram, C.; Viswanathan, N.; Meenakshi, S. Uptake of fluoride by nano-hydroxyapatite/chitosan, a bioinorganic composite. *Bioresour. Technol.* **2008**, *99*, 8226.
(36) Cheng, W.; Zhang, W.; Hu, L.; Ding, W.; Wu, F.; Li, J. Etching synthesis of iron oxide nanoparticles for adsorption of arsenic from water. *RSC Adv.* **2016**, *6*, 15900.

DOI: 10.1021/acs.iecr.6b03856
Ind. Eng. Chem. Res. 2017, 56, 2425−2432